CFD-BASED DESIGN OF EXPERIMENTS FOR THE STUDY OF FLOW-INDUCED VIBRATIONS IN A TUBE BUNDLE

Bárbara Louize da Silva, blsilva1203@hotmail.com
Jonathan Utzig, jutzig@furb.br
Henry França Meier, meier@furb.br
Chemical Engineering Department – University of Blumenau
R. São Paulo, 3250, I-303 – 89030-000 Blumenau – Santa Catarina – Brazil

Abstract. *Flow-induced vibrations (FIVs) are a common problem in many fields of engineering. They originate from the turbulence of the flow and manifest themselves through different mechanisms, which motivate the study of the flow past a single fixed cylinder as a canonical model. The proximity effect of neighbor cylinders has also been investigated, but the flow around a tube bundle and its influence on tube vibrations still demand understanding due to the great number of variables involved. The purpose of this paper is to introduce the first part of a FIV validation study in a confined tube bundle, which is the simulation-based design of an experimental facility. Numerical simulations were carried out using Reynolds-Averaged Navier Stokes (RANS) equations as a qualitative mean of hydrodynamic coefficients and flow patterns evaluation. The coefficients were considered the response variables in a two level full factorial design with the longitudinal and transversal pitch to diameter ratios as factors. The flow characteristics analysis for the four extreme cases in the factorial design revealed that the qualitative approach adopted was sufficient, as flow patterns reported in the literature were identified. The flow patterns observed were related to the mean drag coefficient and root-mean-square value of the lift coefficient of each cylinder in the tube bundle for the considered cases. Statistical and visual analyses show that the transversal spacing ratio is more influentiable on flow regime transition and subsequent changes on hydrodynamic coefficients.*

1. INTRODUCTION

Vibrations are present in every turbulent flow due to the transient nature of the flow forces. They can be beneficial as in the enhancement of heat transfer (Shi *et al*., 2014), but flow-induced vibrations (FIVs) are generally undesired in industrial equipment due to noises, fatigue in the supports and, in most extreme conditions, even the rupture of the structure and leakage, leading to expensive damages (Païdoussis, 2006). Some industrial applications which motivate the study of vibrations caused by the external flow are marine petroleum drilling risers, pressured-water nuclear reactors and tube bundles in heat exchangers and steam generators.

A single circular cylinder subjected to cross-flow has been used as an initial simplified model for the study of the fundamentals and mechanisms of FIVs, especially the ones induced by vortices (Norberg, 2003; Williamson and Govardhan, 2008; Wu *et al.*, 2012). This investigation was expanded for two cylinders, which consists of the smallest cell of a tube bundle. Proximity effects and flow patterns were identified (Sumner, 2010), as well as vortex-induced vibration regimes, depending on the spacing ratio L/D where L is the shortest distance between the cylinders centers and D is the cylinder diameter (Kim *et al*., 2009; Kim and Alam, 2015). Sumner (2010) highlights three main flow patterns for the tandem (one behind the other) and side-by-side arrangements of cylinders. For the tandem arrangement, they are the single bluff-body flow ($1 < L/D < 1.2\sim2$), shear layer reattachment regime ($1.2\sim2 < L/D < 3.4\sim5$) and vortex shedding from both cylinders ($L/D > 3.4\sim5$). For the side-by-side arrangement, the major flow patterns are single bluff-body flow ($1 < L/D < 1.1\sim1.2$), biased vortex streets ($1.1\sim1.2 < L/D < 2\sim2.2$) and parallel vortex streets ($L/D > 2\sim2.2$). For a staggered arrangement, Sumner (2010) classifies the patterns according to the flow incidence angle and spacing ratios.

The flow past two circular cylinders is not yet fully understood, but this study has already been extended for small tube bundles. Lam *et al.* (2008) and Lam and Zou (2010) numerically investigated the flow around four cylinders in an in-line square configuration at low Reynolds numbers for different spacing ratios, respectively in a two-dimensional and three-dimensional domain. Flow patterns similar to the ones described by Sumner (2010) were observed in both cases. Wang *et al.* (2013) reviewed previous published papers on the flow around four cylinders in a square configuration at various spacing ratios and incidence angles, and experimentally investigated the influence of both parameters at a fixed Reynolds number of 8000 in the flow fields, hydrodynamic coefficients and Strouhal number. For the in-line configuration, three flow patterns were observed: shielding regime ($L/D \leq 2$), reattachment regime ($2.5 \leq L/D \leq 3.5$) and impinging regime ($L/D \geq 4$).

Despite the recent progress in the understanding of flow interference and its correlation to fluid forces, which cause FIV in tube bundles, many questions still remain due to the complexity of the flow associated with the number of cylinders. Therefore, a new experiment is proposed to study FIVs in a small fixed tube bundle in a water channel, seeking to observe the separate influence of spacing ratios in the transverse and longitudinal directions at different Reynolds numbers. For this purpose, a qualitative factorial design was carried out to analyze the sensibility of each cylinder in the bundle to the spacing ratio, and to help identifying which configurations will be considered for the

experimental set-up. Each run in the factorial design was accomplished by numerical simulations with RANS equations. Although the results obtained were analyzed mostly in a qualitative way, the flow around a single cylinder was also simulated for comparison with Large Eddy Simulation (LES) results to provide information about the capability of the RANS approach to predict FIVs.

2. MATHEMATICAL MODELS AND METHODS

Even though the flow around bluff bodies is not ideally represented by RANS equations in general (Fröhlich and Von Terzi, 2008; Saltara and Pedrão, 2012), this approach has been chosen due to lower mesh resolution requirements which leads to lower computational costs when compared to LES and other hybrid methods. This is suitable for the qualitative results sought in this paper.

The unsteady RANS or LES equations for the incompressible Newtonian flow may be written according to Eq. (1) and (2), where the symbols $\langle\,\rangle$ denote the average operation for RANS or the filter operation for LES; u_i are the velocity components, x_i are the Cartesian coordinates, ν is the fluid kinematic viscosity, ρ is the fluid density, p is the pressure and τ_{ij} may be the Reynolds turbulent stress tensor for RANS or the subgrid scale stress tensor for LES:

$$\frac{\partial\langle u_i\rangle}{\partial x_i} = 0, \tag{1}$$

$$\frac{\partial\langle u_i\rangle}{\partial t} + \frac{\partial}{\partial x_j}\left(\langle u_i\rangle\langle u_j\rangle\right) = \frac{\partial}{\partial x_j}\left[\nu\left(\frac{\partial\langle u_i\rangle}{\partial x_j} + \frac{\partial\langle u_j\rangle}{\partial x_i}\right)\right] - \frac{1}{\rho}\frac{\partial\langle p\rangle}{\partial x_i} - \frac{\partial\tau_{ij}}{\partial x_j}. \tag{2}$$

For the RANS equations approach, the one-equation eddy viscosity model of Spalart and Allmaras (1992) was chosen to solve the Reynolds turbulent stress tensor, based on the results of Shinde *et al.* (2014) for a two-dimensional simulation of a tube bundle and on initial tests carried out previously. The eddy viscosity (ν_t) is computed from Eq. (3), which introduces a modified eddy viscosity $\tilde{\nu}$ and a viscous damping function f_{v1}, defined by Eq. (4):

$$\nu_t = \tilde{\nu} f_{v1}, \tag{3}$$

$$f_{v1} = \frac{\chi^3}{\chi^3 + C_{v1}^3}, \quad \chi = \frac{\tilde{\nu}}{\nu}. \tag{4}$$

The modified eddy viscosity is calculated from the transport equation shown in Eq. (5), where G_ν is the production of eddy viscosity and Y_ν is the destruction of eddy viscosity. C_{b1}, C_{b2}, C_{v1}, $\sigma_{\tilde{\nu}}$, C_{w1}, C_{w2}, C_{w3} and κ are constants, kept at the default values of Spalart and Allmaras (1992):

$$\frac{\partial\tilde{\nu}}{\partial t} + \frac{\partial}{\partial x_i}(\tilde{\nu}u_i) = G_\nu + \frac{1}{\sigma_{\tilde{\nu}}}\left[\frac{\partial}{\partial x_j}(\nu+\tilde{\nu})\frac{\partial\tilde{\nu}}{\partial x_j} + C_{b2}\left(\frac{\partial\tilde{\nu}}{\partial x_j}\right)^2\right] - Y_\nu, \tag{5}$$

$$G_\nu = C_{b1}\tilde{S}\tilde{\nu}, \quad \tilde{S} = S + \frac{\tilde{\nu}}{\kappa^2 d^2} f_{v2}, \quad f_{v2} = 1 - \frac{\chi}{1+\chi f_{v1}}, \tag{6}$$

$$Y_\nu = C_{w1} f_w \left(\frac{\tilde{\nu}}{d}\right)^2, \quad f_w = g\left(\frac{1+C_{w3}^6}{g^6+C_{w3}^6}\right)^{1/6}, \quad g = r + C_{w2}(r^6 - r), \quad r = \frac{\tilde{\nu}}{\tilde{S}\kappa^2 d^2}. \tag{7}$$

In Eq. (6), S is the scalar norm of the deformation tensor. It was calculated from both vorticity (Ω_{ij}) and strain rate (S_{ij}) tensors, as proposed by Dacles-Mariani *et al.* (1995) to reduce the overprediction of eddy viscosity:

$$S = |\Omega_{ij}| + 2\,min\left(0, |S_{ij}| - |\Omega_{ij}|\right), \tag{8}$$

$$\Omega_{ij} = \frac{1}{2}\left(\frac{\partial u_i}{\partial x_j} - \frac{\partial u_j}{\partial x_i}\right), \quad S_{ij} = \frac{1}{2}\left(\frac{\partial u_j}{\partial x_i} + \frac{\partial u_i}{\partial x_j}\right). \tag{9}$$

For the LES of a single cylinder, the subgrid scale stress tensor was solved with the Smagorinsky model (Smagorinsky, 1963), which also makes use of the eddy viscosity hypothesis:

$$\nu_t = (C_S\Delta)^2|S_{ij}|. \tag{10}$$

In Eq. (10), Δ is the grid filter scale and C_S is the Smagorinsky constant, which needs to be defined by the user. The commonly used value of 0.1 was chosen (Lam *et al.*, 2010).

The three-dimensional model was solved with the finite volume method implemented in the commercial code ANSYS Fluent 14.0 with the physical properties of liquid water (ρ=998.2 kg/m³; ν=1e-6 m²/s) and for different geometries, described as follows.

The domain consists of tube bundle with twelve cylinders confined in a horizontal channel. An in-line array was selected, as it allows for an easier comparison with the flow patterns observed by other authors. To evaluate the effects of proximity and position inside the tube bundle for each cylinder, the spacing ratios in the transversal (H/D) and longitudinal (L/D) directions were appointed as factors in a 2^2 factorial design with one center point. Five cases were, therefore, simulated according to Tab. 1. The high and low levels for each factor were set according to the flow patterns observed by Sumner (2010) and Wang *et al.* (2013) and according to the future experimental set-up operational limitations. The i*th* cylinder's response to the configuration was accounted through the temporal mean drag coefficient $\bar{C}_D$ and the root-mean-square value of the lift coefficient C'_L.

Table 1. Factorial design 2^2.

Case	Factors		Response variables	
	H/D	L/D	$\bar{C}_{D_i}$	C'_{L_i}
A11	1.5	2		
A21	3	2		
A12	1.5	4		
A22	3	4		
AC	2.25	3		

The tube bundle is organized in four rows of three cylinders each, centered in the crosswise direction inside the channel, as illustrated by the AC case in Fig. 1(a). All cylinders, numbered from 01 to 12, have a diameter of 0.01 m. The domain has a streamwise length of 60D, with the upstream boundary 15D away from the first row of cylinders. The domain length was set at 8D in the crosswise direction, and at 3D in the spanwise direction, which was considered enough, based on the domain size of Lam *et al.* (2010). Thus, a blockage ratio of 37.5% was obtained.

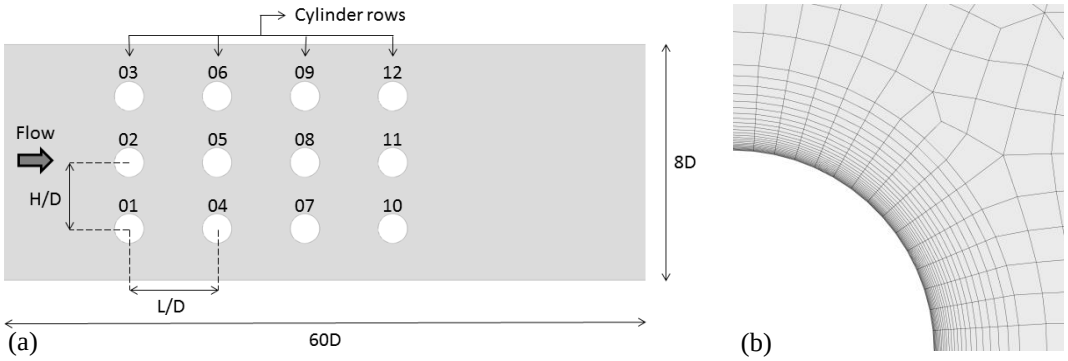

Figure 1. (a) Computational domain for the AC case (out of scale); (b) Detail of the mesh around a cylinder.

A hexahedral grid was generated for each case, with the total number of computational cells ranging from 423,528 to 526,824. Figure 1(b) shows the mesh refinement close to the cylinders surfaces. In all cases, the first grid node distance to the cylinder surface was set as to guarantee a y^+ value inferior to 1.

An uniform inlet velocity of V_{in} = 0.39 m/s was set normal to the entrance surface in Fig. 2, to produce a cylinder Reynolds number of 3900, calculated from Eq. (11). This condition fits in the subcritical regime, where the vortex wake is completely turbulent and transition to turbulence occurs in the free shear layers.

$$Re_D = \frac{V_{in}D}{\nu}. \tag{11}$$

At the outflow, a pressure outlet condition with P = 0 is prescribed. The channel walls, normal to the X axis, were set with a no-slip condition, as well as the cylinders' walls. Finally, a periodic condition was used at the top and bottom surfaces of the domain (which are normal to the Y axis in Fig. 2).

The SIMPLE algorithm was used for pressure-velocity coupling in all cases. Advective and diffusive fluxes were spatially discretized with the second order upwind method and the central differences method, respectively. Gradients were computed with the least squares cell-based method. A non-dimensional time step of $V_{in}\Delta t/D$ = 0.0195 was chosen, which led to maximum Courant numbers that ranged from 1.8 to 2.8, depending on the geometrical arrangement.

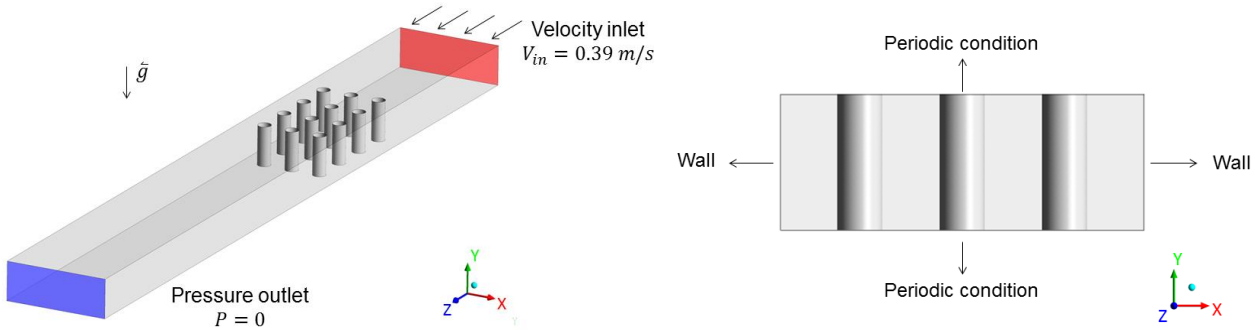

Figure 2. Schematic of the computational domain for the AC case.

3. RESULTS AND DISCUSSION

In this section, a comparison between global parameters of the simulation with the Spalart-Allmaras turbulence model and the LES of the confined flow around a single cylinder is briefly presented. Finally, the flow patterns and hydrodynamic coefficients of each cylinder are analyzed for the spacing ratios considered for the tube bundle described in section 2.

3.1. Single cylinder analysis

The results presented in this paper for the flow around a tube bundle allow for only a qualitative analysis due to the adoption of a RANS equations approach, but it is interesting to observe the difference of this method's results from a previously validated LES method for the flow around a single cylinder at Re_D = 3900 (Silva *et al.*, under revision).

The domain for both LES and Spalart-Allmaras cases consists of a single cylinder inserted in a horizontal channel with the same dimensions shown in Fig. 1(a), except for the length in the spanwise direction. The LES did not make use of the periodic boundary condition simplification and had a spanwise length of 9D, which provides a cylinder aspect ratio AR = 9. The Spalart-Allmaras case was, therefore, carried out with the same domain and boundary condition settings as the LES (other boundaries had the same conditions listed in section 2). Table 2 presents the mean drag coefficient $\bar{C}_D$, the root-mean-square value of the lift coefficient C'_L, the mean recirculation length L_r/D, the mean pressure coefficient at a central point in the back of the cylinder $\bar{C}_{P_{back}}$ and the Strouhal number St for the different approaches. The mean recirculation length is defined as the distance between the cylinder center point and the point where the derivative of the mean streamwise velocity changes sign, and the Strouhal number is given by:

$$St = \frac{f_v D}{V_{in}}, \tag{12}$$

where f_v is the vortex shedding frequency.

Table 2. Global results for the confined flow around a single cylinder.

Turbulence approach	$\bar{C}_D$	C'_L	$-\bar{C}_{P_{back}}$	L_r/D	St
LES Smagorinsky (AR = 9)[(1)]	1.105	0.047	0.714	1.788	0.172
Spalart-Allmaras (AR = 9)	1.413	0.311	1.272	0.715	0.111

[(1)] Silva *et al.*, under revision.

The results of the Spalart-Allmaras case with AR = 9 follow the same behavior as other RANS equations models. For the unconfined flow around a single cylinder at Re_D = 3900 and the k-ω SST model, Luo *et al.* (2014) obtained values of $\bar{C}_D$, $-\bar{C}_{P_{back}}$ and L_r/D respectively 31% higher, 60% higher and 65% lower than experimental results. The differences are close to the ones obtained for the confined flow investigated with the Spalart-Allmaras model when compared to the LES results of Silva *et al.* (under revision), which are 28% higher for $\bar{C}_D$, 78% higher for $-\bar{C}_{P_{back}}$ and 60% lower for L_r/D. The Strouhal number obtained for this case was 35% lower than the LES, and the value of C'_L is appreciably higher, but this discrepancy was not unexpected as even for experimental data there is a great scatter of C'_L values (Wang *et al.*, 2013).

Saltara and Pedrão (2012) presented the same trends for the force coefficients of a SST simulation, when compared to LES and hybrid models results. The authors observe that the unsteady RANS model used cannot capture a great

number of tridimensional structures. This also occurs for the Spalart-Allmaras model, which may be due to the small separation of flow time scale and turbulent scale, assumed in the averaging process of the Navier-Stokes equations (Saltara and Pedrão, 2012).

3.2. Tube bundle flow characteristics

From this section on, all cases were solved with a RANS equations approach and the Spalart-Allmaras model. Instantaneous vorticity contours nondimensionalized by the cylinders diameter D and the inlet velocity V_{in} are shown in Fig. 3 for the four extreme cases A11, A12, A21 and A22 identified in Tab. 1, after 585 nondimensional time units. The shielding flow regime reported by Wang *et al.* (2013) for lower spacing ratios can be clearly identified for the first rows of cylinders in case A11. The shear layers which separate from cylinders 1, 2 and 3 adhere to the cylinders 4, 5 and 6, however, some poorly organized vortex shedding occurs from the first and last cylinders of each row due to the tube bundle's distance from the channel walls.

Case A22 is a result of the combined increase in both spacing ratios H/D and L/D. This case displays the impinging regime, in which the vortices shed from upstream cylinders impinge on downstream cylinders. The same anti-phase relationship found by Wang *et al.* (2013) for the highest spacing ratios was also identified in case 22, where cylinders 1, 2 and 3, for example, shed vortices in alternate sides for each shedding cycle. For the cylinders in the middle of each row (2, 5, 8 and 11), these vortices impinge on downstream cylinders in a synchronized way, which results in the feedback of downstream vortex shedding. The feedback mechanism seems to be damped by the proximity of the walls for the first and last cylinders of each row. The vortices shed from these cylinders interact strongly with the channel walls, apparently extracting vorticity from them. This phenomenon was also numerically observed by Griffith *et al.* (2011) for the confined flow around a single cylinder at low Reynolds numbers.

Case A12 differs from case A11 in the L/D ratio only. Strong proximity effects in the transversal direction can be observed, as vortices shed from cylinders 1 and 3, for example, divert the vorticity after cylinder 2 and dismantle its wake formation. This reproduces the biased flow pattern identified by Sumner (2010) for two side-by-side cylinders, which occurs for every row in the tube bundle. In this pattern, the transversal proximity seems to be restraining vortex shedding when promoting elongated vortices. Due to the wake diversion, the elongated vortices may impinge on neighbor cylinders located obliquely, and no feedback mechanism occurs. The strongest vortices are the free ones shed by the cylinders at the ends of each row.

Case A21 allows for the analysis of longitudinal proximity. The contours in Fig. 3 show that transversal proximity had greater influence at keeping the shielding flow pattern in case A11, as in case A22 both reattachment and impinging regimes being apparent. Shear layer reattachment happens especially for the first cylinder rows; in this instant it is visible after cylinders 1 and 2 for negative vorticity and after cylinders 4 and 5 for positive vorticity. Discrete vortices can also be observed, for example after cylinders 8 and 9. Again, vortices shed from the first and last cylinders of each row interact with the channel walls.

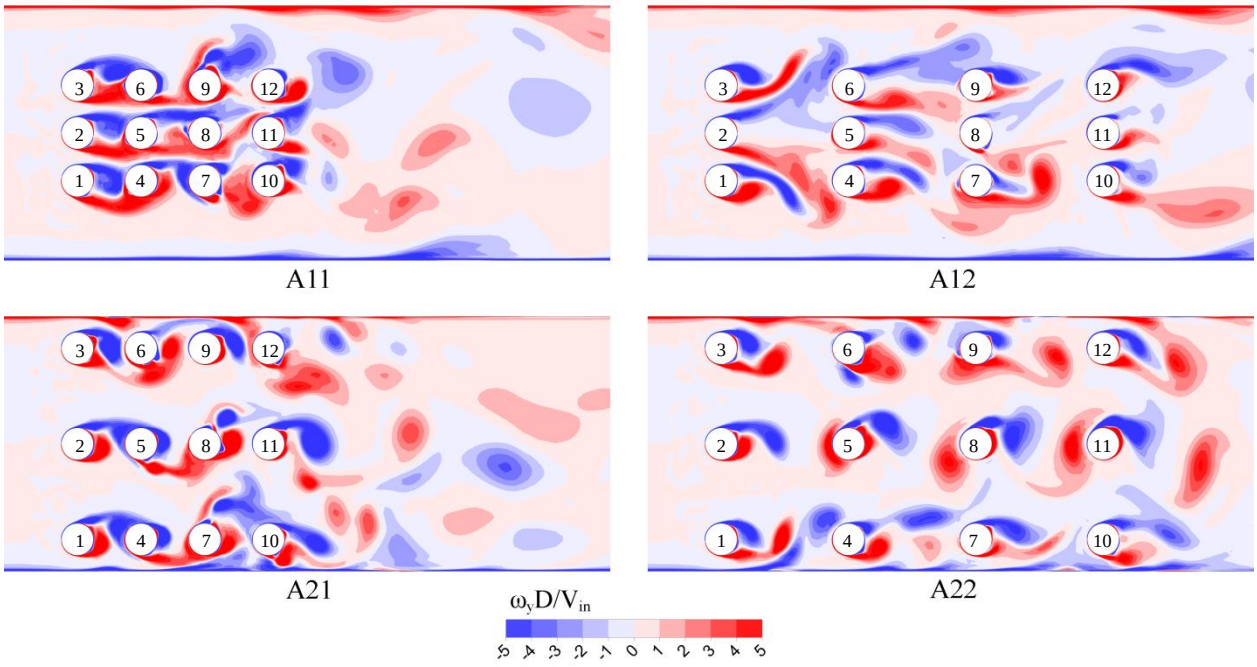

Figure 3. Instantaneous nondimensional vorticity contours for the cases A11, A12, A21 and A22.

3.3. Hydrodynamic coefficients and statistical analysis

The flow patterns observed in the previous section reflect on the drag and lift coefficients of each cylinder. These coefficients were submitted to a statistical analysis of variance with a significance level of 10% to avoid type II errors, which is failing to detect present effects, following the factorial design presented in Tab. 1. The analysis shows that for almost all variables, no factor was statistically significant, but major trends identified in the statistical predictions can be related to the flow characteristics.

Figure 4 presents the mean drag coefficient $\bar{C}_D$ of each cylinder for the cases A11, A12, A21 and A22, where the circle area is related to the magnitude of $\bar{C}_D$. The first cylinder row has similar values in every arrangement, 35% to 70% higher than the coefficient for a single cylinder with the periodic condition (see Tab. 2). Wang *et al.* (2013) obtained values up to 25% higher in their experiment. For the A11 and A12 cases, i.e. the ones with lower transversal spacing ratios, all other cylinders have lower values of $\bar{C}_D$, which is also in accordance with the results of Wang *et al.* (2013) and Lam and Zou (2010). This is related to the weak vortex shedding that occurs at these spacing ratios, which explains why the cylinders at the ends of the downstream rows (with the exception of cylinder 6 in A12 case) have slightly higher values of $\bar{C}_D$ than their neighbors in the middle. For both A21 and A22 cases, i.e. the ones with higher transversal spacing ratios, cylinder 8 is the one with the highest value of $\bar{C}_D$ in the tube bundle. For the cylinders in the middle of each row, the mean drag coefficient experiences a decrease at cylinder 5, followed by an increase at cylinder 8 and a decrease at cylinder 11. In all rows, the value for the middle cylinder $\bar{C}_D$ is higher than the ones at the ends of the row, unlike what happened for cases A11 and A12.

Increasing the longitudinal spacing ratio L/D caused an increase in the value of $\bar{C}_D$ for the middle cylinders, with the exception of cylinder 2 in the A12 case. Wang *et al.* (2013) observed that, for higher spacing ratios, the value of $\bar{C}_D$ increased monotonically for the downstream cylinders, but for the upstream cylinders it first suffered a decrease followed by an increase. Overall, the spacing ratio H/D had a greater influence than L/D on the behavior of $\bar{C}_D$. This was also shown by the statistical analysis: the effects of L/D are more noticeable than H/D only for cylinders 1 and 3.

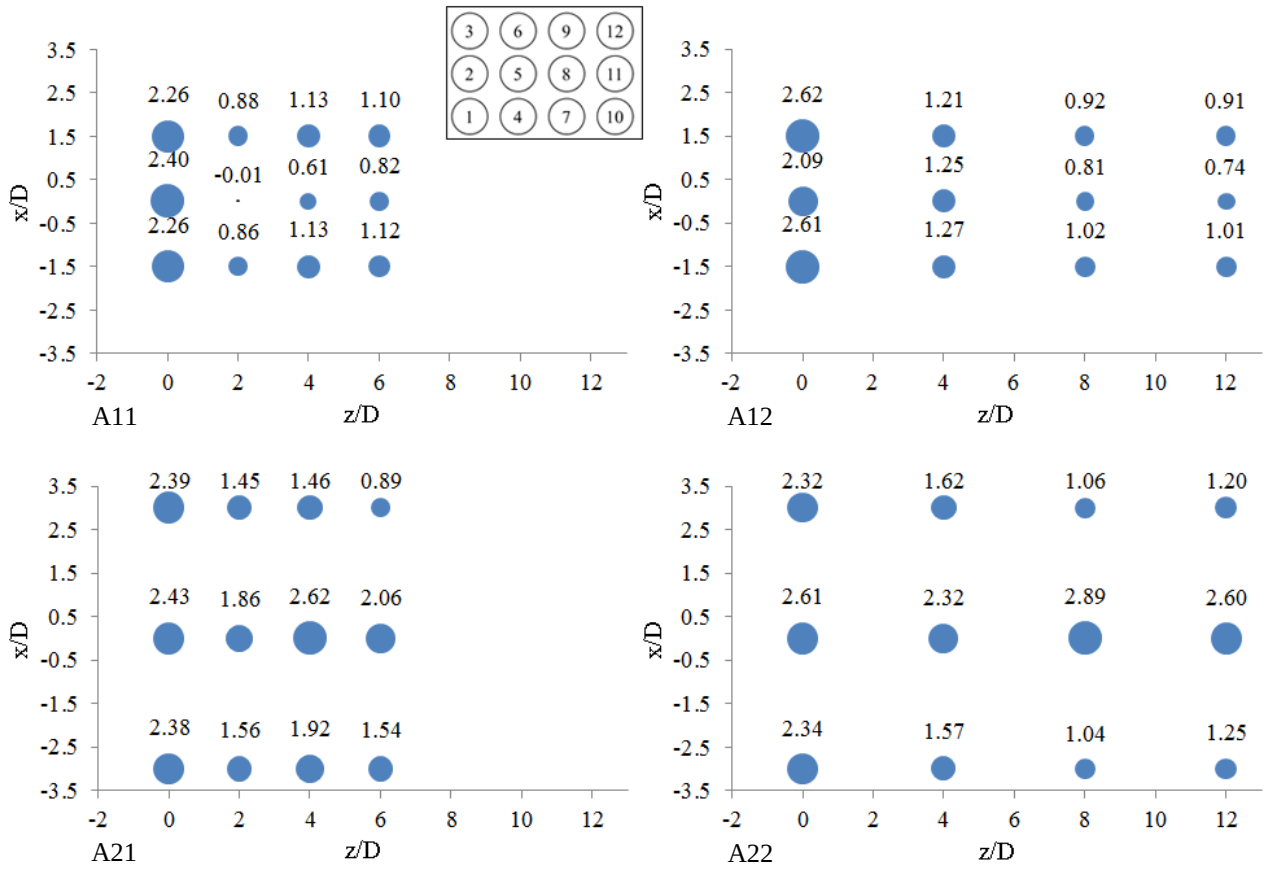

Figure 4. Mean drag coefficient for each cylinder in the arrangements A11, A12, A21 and A22.

Figure 5 shows the root-mean-square value of the lift coefficient C_L' of each cylinder for the cases A11, A12, A21 and A22. In this figure, the circle size is related to the magnitude of C_L'. For the A11 and A12 cases, in every row the value of this coefficient is lower for the middle cylinder. It was expected due to the flow patterns described in section

3.2, that favor vortex shedding from the cylinders at the ends of each row in the tube bundle. The difference of C_L' between the middle cylinder and the end ones for downstream rows is attenuated in case A12, which is attributed to the non-occurrence of the feedback mechanism described previously.

Case A21 features an increase of C_L' for the second row of cylinders in every position. In the third row this trend continues for the coefficient of the middle cylinder, which becomes higher than the values for the cylinders at the ends of the row. This may be due to cylinder 8's distance from the wall when compared to its neighbors, which promotes a less chaotic vortex shedding behavior. In the fourth row, C_L' declines for all cylinders. The distribution of C_L' in case A22 is similar to the one in case A21, however, there is an increase in C_L' for all cylinders at the fourth row. The feedback mechanism acting for the middle cylinders is clear, as C_L' continuously rises.

The results obtained for the first two rows in all cases agree with the ones from Wang *et al.* (2013) and Lam and Zou (2010), who reported higher values of C_L' for the downstream cylinders, when compared to upstream cylinders, and a growth of C_L' with the spacing ratio. The statistical analysis reinforced that the spacing ratio H/D had more influence than L/D for the cylinders in the middle of each row, but cylinders 7, 9, 10 and 12 were more affected by L/D.

It remains to be found, however, whether the patterns and mechanisms identified for both $\bar{C}_D$ and C_L' in each arrangement carry on for tube bundles with more cylinders. Further studies would be necessary to confirm or present new behaviors.

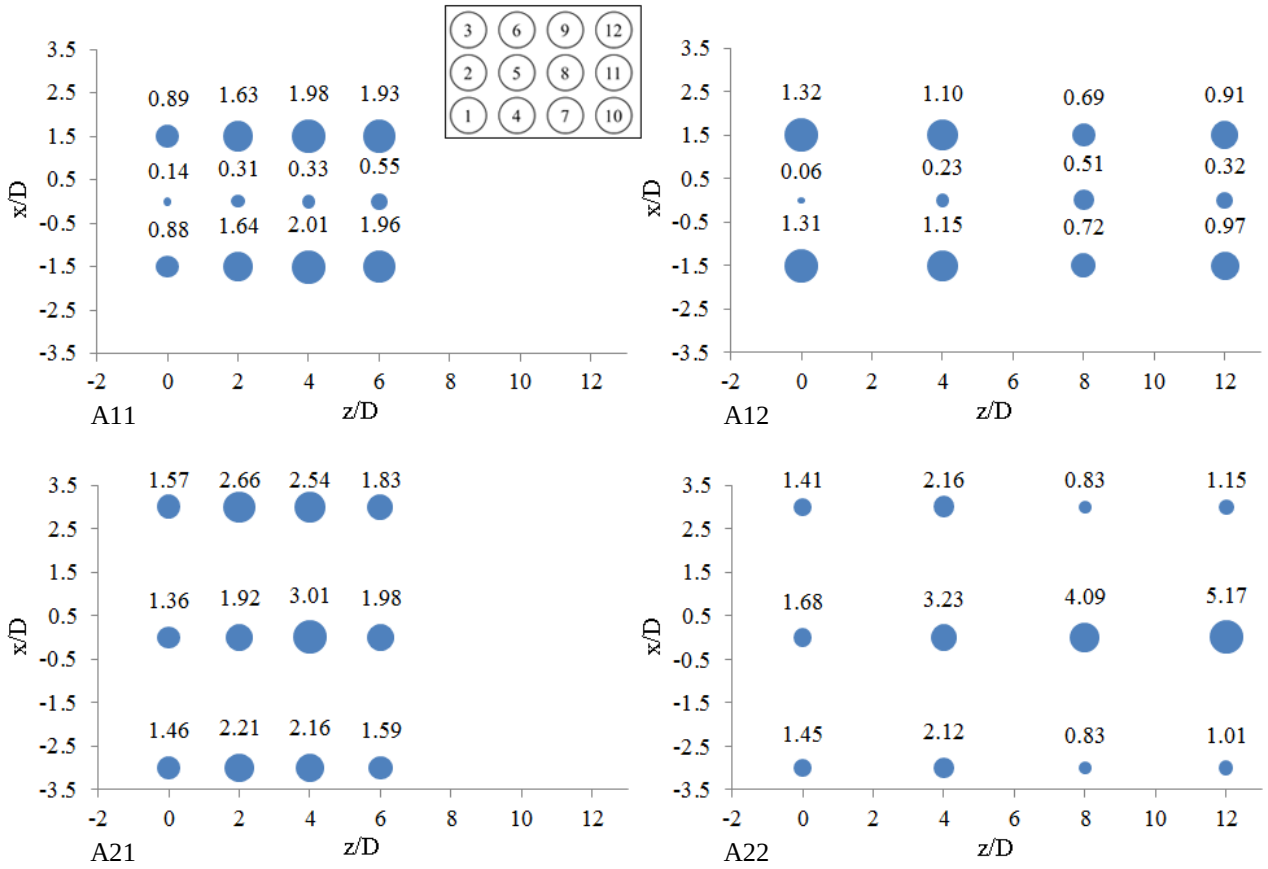

Figure 5. Root-mean-square value of the lift coefficient for each cylinder in the arrangements A11, A12, A21 and A22.

4. CONCLUSIONS

A simulation-based design of experiments at a fixed Reynolds number was carried out to aid in the design of a new experimental facility to study FIVs. The RANS equations approach allowed for a qualitative analysis of the separate influence of transversal and longitudinal spacing ratios in the flow characteristics and hydrodynamic coefficients, for an in-line tube bundle confined in a horizontal channel.

Flow regimes reported by other authors for two cylinders or smaller tube bundles were identified in the four extreme cases of the factorial design and related to the cylinders' respective mean drag coefficient and root-mean-square value of the lift coefficient. It was found that the transversal spacing ratio had more influence than the longitudinal spacing ratio on flow regime transition, which is linked to greater effects of the transversal spacing ratio on the hydrodynamic coefficients evaluated for the middle cylinders.

Trends observed for the hydrodynamic coefficients still need to be confirmed for larger tube bundles, but this study may aid in the solution of FIVs in industrial equipment such as steam generators by enabling the identification of weaker points in the bundle, or suggesting more favorable arrangements to mitigate FIVs in the equipment design. Future experiments and more accurate numerical simulations will be carried out to verify the separate influence of each spacing ratio, guided by the results presented.

5. ACKNOWLEDGEMENTS

The authors would like to acknowledge the financial support from Petróleo Brasileiro S.A. (PETROBRAS) through the cooperation agreement 0050.0070 334.11.9 and the National Counsel of Technological and Scientific Development (CNPq), process 310504/2012-0.

6. REFERENCES

Dacles-Mariani, J., Zilliac, G.G., Chow, J.S. and Bradshaw, P., 1995, "Numerical/Experimental Study of a Wingtip Vortex in the Near Field", AIAA J., Vol. 33, No. 9, pp.1561-1568.

Fröhlich, J. and Von Terzi, D., 2008, "Hybrid LES/RANS methods for the simulation of turbulent flows", Prog. Aerosp. Sci., Vol. 44, pp. 349-377.

Griffth, M.D., Leontini, J., Thompson, M.C. and Hourigan, K., 2011, "Vortex shedding and three-dimensional behaviour of flow past a cylinder confined in a channel", J. Fluid Struct., Vol. 27, pp. 855-860.

Kim, S., Alam, M.M., Sakamoto, H. and Zhou, Y., 2009, "Flow-induced vibrations of two circular cylinders in tandem arrangement. Part 1: Characteristics of vibration", J. Wind Eng. Ind. Aero., Vol. 97, pp. 304-311.

Kim, S. and Alam, M.M., 2015, "Characteristics and suppression of flow-induced vibrations of two side-by-side circular cylinders", J. Fluid Struct., Vol. 54, pp. 629-642.

Lam, K., Gong, W.Q. and So, R. M. C., 2008, "Numerical simulation of cross-flow around four cylinders in an in-line square configuration", J. Fluid Struct., Vol. 24, pp. 34-57.

Lam, K. and Zou, L., 2010, "Three-dimensional numerical simulations of cross-flow around four cylinders in an in-line square configuration", J. Fluid Struct., Vol. 26, pp. 482-502.

Lam, K., Lin, Y.F., Zou, L. and Liu, Y., 2010, "Experimental study and large eddy simulation of turbulent flow around tube bundles composed of wavy and circular cylinders", Int. J. Heat Fluid Fl., Vol. 31, pp. 32-44.

Luo, D., Yan, C., Liu, H. and Zhao, R., 2014, "Comparative assessment of PANS and DES for simulation of flow past a circular cylinder", J. Wind Eng. Aerodyn., Vol. 134, pp. 65-77.

Norberg, C., 2003, "Fluctuating lift on a circular cylinder: review and new measurements", J. Fluid Struct., Vol. 17, pp. 57-96.

Païdoussis, M. P., 2006, "Real-life experiences with flow-induced vibration", J. Fluid Struct., Vol. 22, pp. 741-755.

Saltara, F. and Pedrão, N., 2012, "Comparação entre simulações LES e URANS para escoamentos ao redor de corpos rombudos", Turbulência, Vol. 8, Ed. ABCM, S. Paulo, Brazil, pp. 17-55.

Shi, J., Hu, J., Schafer, S.R. and Hen, C.L., 2014, "Numerical study of heat transfer enhancement of channel via vortex-induced vibration", Appl. Therm. Eng., Vol. 70, pp. 838-845.

Shinde, V., Marcel, T., Hoarau, Y., Deloze, T., Harran, G., Baj, F., Cardolaccia, J., Magnaud, J.P., Longatte, E., Braza, M., 2014, "Numerical simulation of the fluid-structure interaction in a tube array under cross flow at moderate and high Reynolds number", J. Fluid Struct., Vol. 47, pp. 99-113.

Silva, B.L., Utzig, J. and Meier, H.F., under revision, "Vibrações induzidas por escoamento: Avaliação de modelos LES e RANS para escoamento cruzado sobre um corpo cilíndrico", Proceedings of the 21st Brazilian Congress of Chemical Engineering, Fortaleza, Brazil.

Smagorinsky, J., 1963, "General circulation experiments with the primitive equations I, the basic experiment", Mon. Weather Rev., V. 91, pp. 99-165.

Spalart, P.R. and Allmaras, S.R., 1992, "A one-equation turbulence model for aerodynamic flows", AIAA, paper 439.

Sumner, D., 2010, "Two circular cylinders in cross-flow: A review", J. Fluid Struct., Vol. 26, pp. 849-899.

Wang, X.K., Gong, K., Liu, H., Zhang, J.-X. and Tan, S.K., 2013, "Flow around four cylinders arranged in a square configuration", J. Fluid Struct., Vol. 43, pp. 179-199.

Williamson, C.H.K. and Govardhan, R., 2008, "A brief review of recent results in vortex-induced vibrations", J. Wind Eng. Ind. Aero., Vol. 96, pp. 713-735.

Wu, X., Ge, F. and Hong, Y., 2012, "A review of recent studies on vortex-induced vibrations of long slender cylinders", J. Fluid Struct., Vol. 28, pp. 292-308.

7. RESPONSIBILITY NOTICE

The authors are the only responsible for the printed material included in this paper.